ACS NANO

www.acsnano.org

ARTICLE

Electric Field Induced Wetting of a Hydrophobic Gate in a Model Nanopore Based on the 5-HT$_3$ Receptor Channel

Gianni Klesse, Stephen J. Tucker,* and Mark S. P. Sansom*

Cite This: https://dx.doi.org/10.1021/acsnano.0c04387

Read Online

ACCESS | Metrics & More | Article Recommendations | Supporting Information

ABSTRACT: In this study we examined the influence of a transmembrane voltage on the hydrophobic gating of nanopores using molecular dynamics simulations. We observed electric field induced wetting of a hydrophobic gate in a biologically inspired model nanopore based on the 5-HT$_3$ receptor in its closed state, with a field of at least ∼100 mV nm^{-1} (corresponding to a supra-physiological potential difference of ∼0.85 V across the membrane) required to hydrate the pore. We also found an unequal distribution of charged residues can generate an electric field intrinsic to the nanopore which, depending on its orientation, can alter the effect of the external field, thus making the wetting response asymmetric. This wetting response could be described by a simple model based on water surface tension, the volumetric energy contribution of the electric field, and the influence of charged amino acids lining the pore. Finally, the electric field response was used to determine time constants characterizing the phase transitions of water confined within the nanopore, revealing liquid−vapor oscillations on a time scale of ∼5 ns. This time scale was largely independent of the water model employed and was similar for different sized pores representative of the open and closed states of the pore. Furthermore, our finding that the threshold voltage required for hydrating a hydrophobic gate depends on the orientation of the electric field provides an attractive perspective for the design of rectifying artificial nanopores.

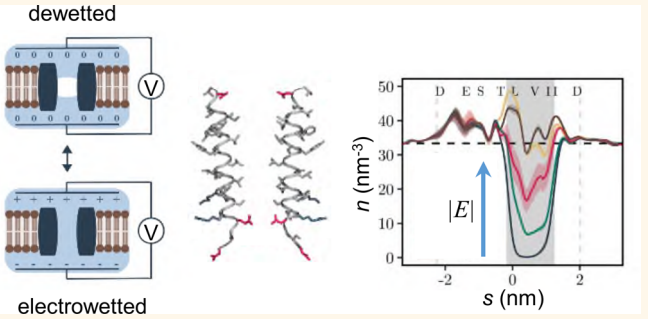

KEYWORDS: *nanopore, ligand gated ion channel, membrane, water, molecular dynamics, hydrophobic gating*

Nanopores enable the permeation of water and small molecules through membranes that separate aqueous compartments. The size of these permeant molecules is typically comparable to the diameter of the pores involved (≤1 nm). Consequently, any interaction of the permeant molecules with the lining of the pores will determine the functional properties of the permeation process.[1−4] In biological membranes, ion channels are structurally dynamic protein nanopores that switch between functionally open and closed conformations to control the rapid permeation of ions and water across the membrane.[5,6] However, when open, a typical channel pore has an internal radius of ∼0.5 nm and a length of ∼5 nm that creates a nanoconfined environment where the precise shape and related dynamic physicochemical properties of the pore will also influence the complex behavior of water and of ions, and therefore their permeation across the membrane. For example, we have previously shown how ion permeation can be influenced by both the pore radius and the local hydrophobicity of the pore lining.[7−9] In such cases, the presence of the band of hydrophobic amino acid side chains lining a pore can induce a local liquid-to-vapor phase transition resulting in that section becoming devoid of liquid water. Such pore "dewetting" creates a free energy barrier for ion permeation. Thus, although ion permeation can occur through polar regions only just wider than the radius of the permeating ion, a hydrophobic region of comparable dimensions can prevent ion permeation without complete steric occlusion of the pore. This process has been referred to as hydrophobic gating and has enhanced our understanding of the mechanisms which control ion permeation through biological ion channels and synthetic nanopores.[10−14]

Received: May 26, 2020
Accepted: July 16, 2020
Published: July 16, 2020

The gating or regulation of hydrophobic gates in ion channels is thought to involve either structural changes in pore radii or more subtle changes in hydrophobicity through, *e.g.*, the rotation of helices that contain side chains of different polarities, and examples of such a hydrophobic gating mechanism have now been proposed in a variety of different channels[13,15−28] and synthetic nanopores.[29,30] However, nearly all biological membranes experience a potential difference of between 50 to 200 mV across them and molecular dynamics (MD) simulations of simple model nanopores show that application of a transmembrane electric field can hydrate an otherwise dewetted hydrophobic constriction, which is thus rendered ion permeable.[31,32] This electrowetting effect can be explained by incorporating the electrical energy of the pore volume element which is wetted into a simple thermodynamic model of gating (see eq 1 below[8]). In addition to this model, which assumes bulk water properties, a number of MD studies have explored the effects of an externally applied electric field on water molecules in nanoconfined hydrophobic environments.[4] For example, simulations of water nanodroplets on hydrophobic surfaces[33] reveal that an electric field modifies the interfacial tension of a nanodroplet by influencing the orientation and hydrogen bonding structure of water molecules located on the droplet surface. Furthermore, MD simulations of water in planar hydrophobic confinement[34] also reveal that interfacial tensions decrease upon application of an electric field, alongside a field-induced change in the average number of hydrogen bonds formed by interfacial water molecules. Electrowetting has also been observed experimentally for several types of artificial biomimetic nanopores.[35] For example, it has been shown that hydrophobic nanopores in polyethylene terephthalate membranes can be wetted and functionally opened through the application of an electric field.[29]

For biological ion channels, the role of electrowetting is even less well understood; most studies have been limited to MD simulations, demonstrating that the dewetted hydrophobic gate of the MscS channel can hydrate when a transmembrane voltage of between 0.25 and 1.2 V is applied.[36,37] Comparable electrowetting of a hydrophobic gate in a model protein nanopore has been simulated,[38] and electrowetting has also been seen within the hydrophobic pores formed by carbon nanotubes.[39] However, while it is clear that electrowetting can in principle open a hydrophobic gate, a detailed quantitative relationship between pore hydration probability and the applied electric field has not so far been examined for a biologically realistic model of an ion channel. It therefore remains unclear how such effects of electric fields depend on the structure of the pore and the strength of the applied field or how robust such predictions are to variations in the precise type of water model used in the MD simulations. It is therefore important that these effects are captured by a theoretical model which may subsequently be used in a quantitative predictive fashion.

In this study we have examined the effects of an applied electric field on a hydrophobic gate within a model protein nanopore derived from the transmembrane pore of the 5-HT_3 receptor, a biologically relevant ion channel distributed throughout the central nervous system.[40] Our results demonstrate that an electric field can induce wetting of the hydrophobic gate in this model nanopore, at values that correspond to a (supra-physiological) transmembrane potential difference of ∼1 V. A simple thermodynamic model can be used to quantitatively describe the increase in pore hydration probability with increasing electric field. Interestingly, the observed asymmetry of the hydration probability response curve can also be accounted for by the intrinsic electric field generated by the distribution of charged amino acid residues along the length of the nanopore which provides an attractive perspective for the design of intrinsically rectifying artificial nanopores.

RESULTS AND DISCUSSION

Model Nanopore Based on the 5-HT_3 Receptor. To quantify the effects of electrowetting of a hydrophobic gate, we have employed MD simulations of the M2 helix nanopore which corresponds to the pore lining segment of the 5-HT_3 receptor channel.[19] This model nanopore forms an ideal system for studying hydrophobic gating because it embodies many aspects of the wetting/dewetting behavior observed in complex ion channel proteins,[41] while remaining sufficiently simple to allow functional dissection by an extended series of atomistically detailed simulations (Figure 1).[42]

To evaluate our expectation that the model nanopore can capture the hydration state behavior of the larger parent channel protein, we compared simulations (3 × 50 ns) of the complete 5-HT_3 receptor in closed (PDB ID: 4PIR)[43] and open (PDB ID: 6DG8)[19] states with simulations (3 × 150 ns) of the corresponding model nanopores. In the latter simulations, only the pore-lining M2 helices of the channel were included. Both the complete protein channel and the model nanopores were embedded in a phospholipid bilayer and solvated in an ∼0.15 M NaCl electrolyte using the mTIP3P water model.

These simulations show that, in the absence of an electric field, the resulting water density profiles (Figure 1B) through the transmembrane pore regions are nearly identical for the complete channel and for the nanopore simulation systems. In both cases, the closed state (PDB ID: 4PIR) conformation that had previously exhibited significant dewetting[41] still favors the vapor state even when only the M2 helix nanopore is simulated. In the open conformation (PDB ID: 6DG8), the time-averaged water density in the hydrophobic gate region of the M2 helix nanopore falls slightly below the value observed for the complete channel structure, reflecting the fact that the M2 helix nanopore intermittently dewets. However, the average water density remains close to the bulk value in these simulations, suggesting the influence of the structural model on the hydration equilibrium is limited and not sufficiently strong enough to bias an otherwise hydrated channel toward the vapor state. These results therefore provide confidence these different conformations of the M2 helix nanopore can be used as a suitable model system to quantify the relationship of the pore radius, electric field, and water model in the electrowetting and conductance behavior of a biologically relevant nanopore.

MD Simulations of the Model Nanopore in an Electric Field. We therefore examined the effect of an electric field on the liquid−vapor equilibrium that exists within the hydrophobic barrier of the M2 helix nanopore that is based on the closed state structure of the 5-HT_3 receptor (PDB ID: 4PIR)[43] (Figure 2A). Without an electric field, this nanopore remained dewetted throughout most of a 150 ns long simulation (as seen previously[41]) and only entered the wetted state for a small number of very brief periods (Figure 2B). Correspondingly, the time-averaged water density profile (Figure 2C) demonstrates that the hydrophobic gate is primarily devoid of bulk

https://dx.doi.org/10.1021/acsnano.0c04387
ACS Nano XXXX, XXX, XXX−XXX

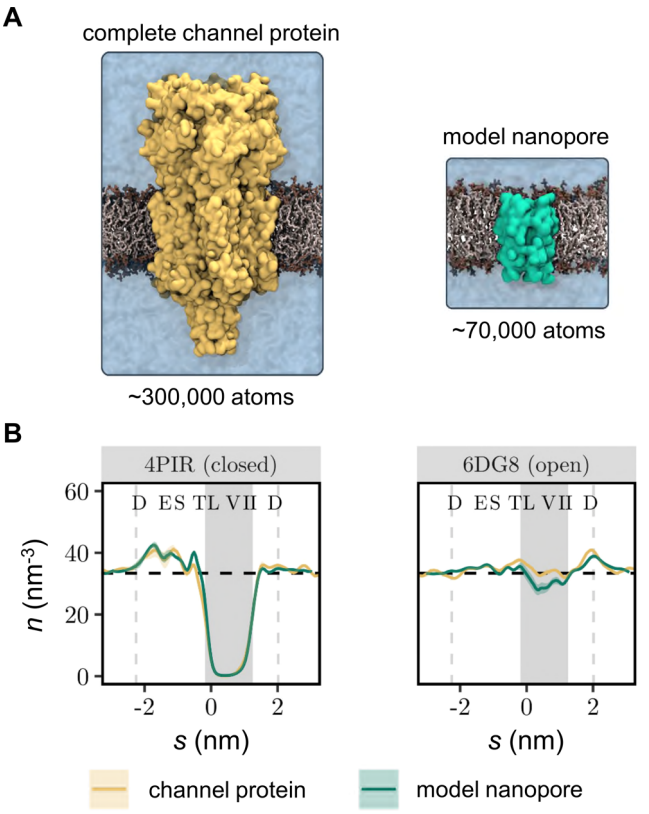

Figure 1. Influence of the nanopore structural model on hydrophobic gating. (A) Simulation system based on the complete 5-HT$_3$ receptor structure (~300 000 atoms for the protein, bilayer, and solution) compared to a much smaller simulation system (~70 000 atoms) based on the M2 helix bundle nanopore. Both structures represent the closed state (PDB ID: 4PIR) of the channel. (B) Time-averaged water density profiles of the complete channel protein (yellow lines) compared with the M2 helix nanopores (green line) compared for a closed state and open state of the 5-HT$_3$ receptor. Water density profiles were determined using a kernel density estimator as described in ref 85 using a bandwidth parameter of 0.14 nm and a time step of 100 ps. Results from three independent repeats were subsequently averaged to derive the mean and standard deviation of the water density shown in the figure. Vertical dashed lines indicate the extent of the M2 helix bundle pore. The shaded background represents the hydrophobic gate region, while the dashed horizontal line represents the density of bulk water (33.37 nm^{-3}). The confidence bands represent the standard deviation over three independent MD simulations.

phase water and exists in a vapor state. When an electric field of ±100 mV/nm was imposed (using the methods described by, *e.g.*, refs 44−46) the channel exhibited frequent liquid−vapor oscillations (Figure 2B). In this situation, the time-averaged density of water in the hydrophobic gate adopts an intermediate value between the dewetted and the hydrated channels (Figure 2C). However, it is important to note the relationship between the units of field strength (i.e., mV/nm) used here to describe the external electric field with the values of transmembrane potential commonly measured experimentally (i.e., mV). In our simulation system, a field strength of 100 mV/nm that induces wetting in this pore (see Figure 2) corresponds to a potential difference ΔV of ~0.85 V across the membrane; this is calculated from $\Delta V = -EL_z$, where E is the external field imposed along the z axis of a simulation box of dimension L_z, as discussed in ref 47. Therefore, if, *e.g.*, the box dimension L_z was doubled the transmembrane voltage ΔV would be doubled. Notably, a value of ΔV = 0.85 V across the membrane is almost an order of magnitude greater than the typical transmembrane voltages experienced physiologically (~0.1 V).

Interestingly, we also observed that a field strength of −100 mV/nm (i.e., one in which the intracellular face of the membrane is at a negative potential relative the extracellular face; Figure 2A) has a greater effect than a field of +100 mV/nm, indicating that the hydration probability of the pore can depend on the direction of the electric field as well as on its magnitude. At higher magnitude electric fields of ±200 mV/nm, the channel pore exists almost exclusively in the wetted state irrespective of field direction (Figure 2B) and the average water density approaches that of bulk water (Figure 2C).

An external electric field can therefore be used to control the phase behavior of nanoconfined water within a biological nanopore by influencing the relative probability of the liquid and vapor states. The probability distribution of the minimal water density is bimodal (Figure 2D; SI Figure S1), and hence the underlying free energy landscape has two minima (as discussed previously[4,7,48]), with one peak near zero and a second peak near the density of bulk water. We note that this figure shows an estimate of the water density in the hydrophobic gate region aggregated over time and the electric field strength. This demonstrates clearly (by aggregating across all field strengths) that the probability distribution of the water density is bimodal, with intermediate density values observed only very rarely. Importantly, this legitimizes our theoretical treatment of the system using a two-state model.

Dependence of the Hydration Probability on the Electric Field. The response of the time averaged pore hydration probability, $\langle\omega\rangle$, to an external electric field, E, was compared for the M2 bundle nanopore in conformations corresponding to closed (PDB ID: 4PIR)[43] and open (PDB ID: 6DG8)[19] states of the 5-HT$_3$ receptor. The hydration behavior of the nanopore was also compared for four different water models (Figure 3). For the closed state, the hydration probability vs E response curve is sigmoidal: the hydration probability is near zero in the absence of a field, increasing to a value of one at fields of high magnitude. The threshold for hydration also varies. For example, with the mTIP3P water model[49] (which is widely used) pore wetting is observed at a field strength which is ~50 mV/nm weaker than with any of the other models (including TIP4P/2005[50] which reproduces well a wide range of properties of water over temperatures from 123 to 573 K and for pressures up to 40 000 bar). However, once pore wetting begins, the transitional regime of intermediate hydration occurs within a further increase of ~100 mV/nm for all four water models. In the case of the open state structures, the response of hydration probability still resembles a (double) sigmoid, but hydration probability does not start at zero, because the pore is already partially hydrated even in the absence of an electric field.

It is important to point out that in the transitional regime the rate of increase in hydration probability appears similar for both positive and negative electric fields, irrespective of the water model. However, the overall curve is shifted toward the right, which makes it asymmetric with respect to E = 0. This is most clearly seen for the closed state, where the threshold voltage for the onset of pore hydration is ~25 mV/nm higher at positive fields than for negative fields. Due to the smaller

https://dx.doi.org/10.1021/acsnano.0c04387
ACS Nano XXXX, XXX, XXX−XXX

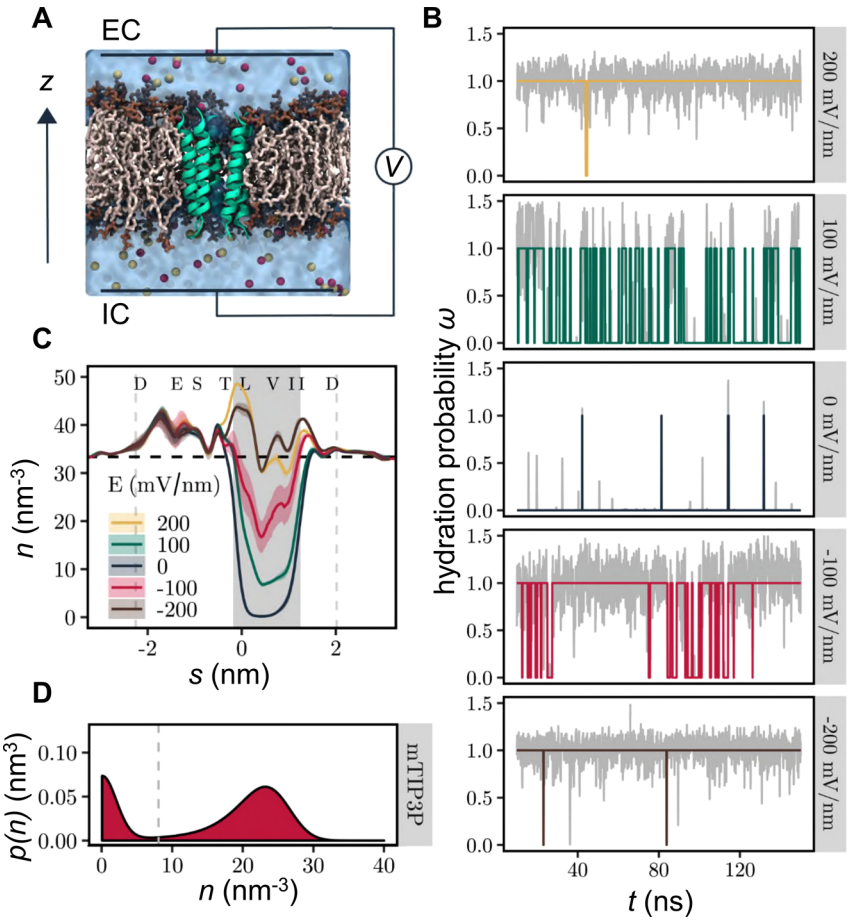

Figure 2. Electrowetting of the hydrophobic gate in the nanopore. (A) The M2 helix bundle nanopore (green) is embedded in a lipid bilayer (brown). Water is represented as a transparent surface, and Na^+ and Cl^- ions are shown as red and yellow, respectively. The effect of a transmembrane potential is modeled by applying a constant electric field to all atomic charges in the system. The transmembrane voltage is reported as $V_{IC} - V_{EC}$ where IC = intracellular (negative z) and EC = extracellular (positive z). (B) Time series of hydration probability (ω) at five different electric field strengths. The gray line in the background represents the minimum water density in the hydrophobic gate normalized to the density of bulk water. The colored lines represent discretization of this via a threshold crossing algorithm (see D below). (C) Time-averaged water density profiles as a function of electric field strength. Confidence bands represent the standard deviation over three independent repeats. The shaded background and vertical dashed lines indicate the extent of the hydrophobic gate and transmembrane domain, respectively. The horizontal dashed line represents the density of bulk water. (D) Kernel density estimate of the water density in the hydrophobic gate region aggregated over time and electric field strength. The dashed gray line indicates the threshold density for classifying the state of the channel as closed, $\omega(t) = 0$, or open, $\omega(t) = 1$. Data shown are based on simulations of the M2 helix nanopore in the closed state using the mTIP3P water model.

number of data points in the dewetted regime, this effect is not as clear for the open state, although, consistent with this effect, the minimum point of the pore hydration probability curve appears shifted to slightly positive fields.

The probability of hydration of a nanopore in the absence of an E-field can be described by

$$\langle\omega\rangle = \frac{1}{1 + \exp(-\beta\Delta\Omega_0)} \quad (1)$$

where $\langle\omega\rangle$ = the time-averaged hydration probability, $\Delta\Omega_0 = \Omega_V - \Omega_L$, *i.e.*, the difference between the free energies of the liquid and vapor states in the absence of an E-field, and $\beta = 1/k_BT$.[7,11] When $\Delta\Omega_0 < 0$, the pore is hydrophobic and favors a vapor state, but when $\Delta\Omega_0 > 0$, the liquid (i.e., hydrated) state is favored. To include the effect of the electric field, E, the free energy term[31] can be modified giving

$$\langle\omega\rangle = \frac{1}{1 + \exp[-\beta(\Delta\Omega_0 + m(E - E_{INT})^2)]} \quad (2)$$

where m denotes the strength of the coupling between hydration probability and the magnitude of the field and E_{INT} accounts for the horizontal offset of the response curve in terms of an intrinsic electric field arising from the nanopore structure (see below). The value of m represents the difference in ability to store electrical energy in a water-filled high-permittivity space vs an empty low-permittivity space, and this is related *inter alia* to the wettable volume of the pore as well as the local dielectric constant of the water model. As can be seen from Figure 3, this model is in good agreement with the simulation data.

Model parameters are given Table 1 (with errors estimated from the Bayesian posterior distributions shown in SI Figure S3). These parameters enable a quantitative analysis of the effects of E-field strength, nanopore conformation, and water model on the hydration probability of the channel. Thus, the zero-field free energy difference is close to zero across all water models for the open state structure with the mTIP3P water model slightly favoring the liquid state by ~1 k_BT, while the

https://dx.doi.org/10.1021/acsnano.0c04387
ACS Nano XXXX, XXX, XXX−XXX

$$\langle\omega\rangle = \frac{1}{1 + exp[-\beta(\Delta\Omega_0 + m(E - E_{INT})^2)]}$$

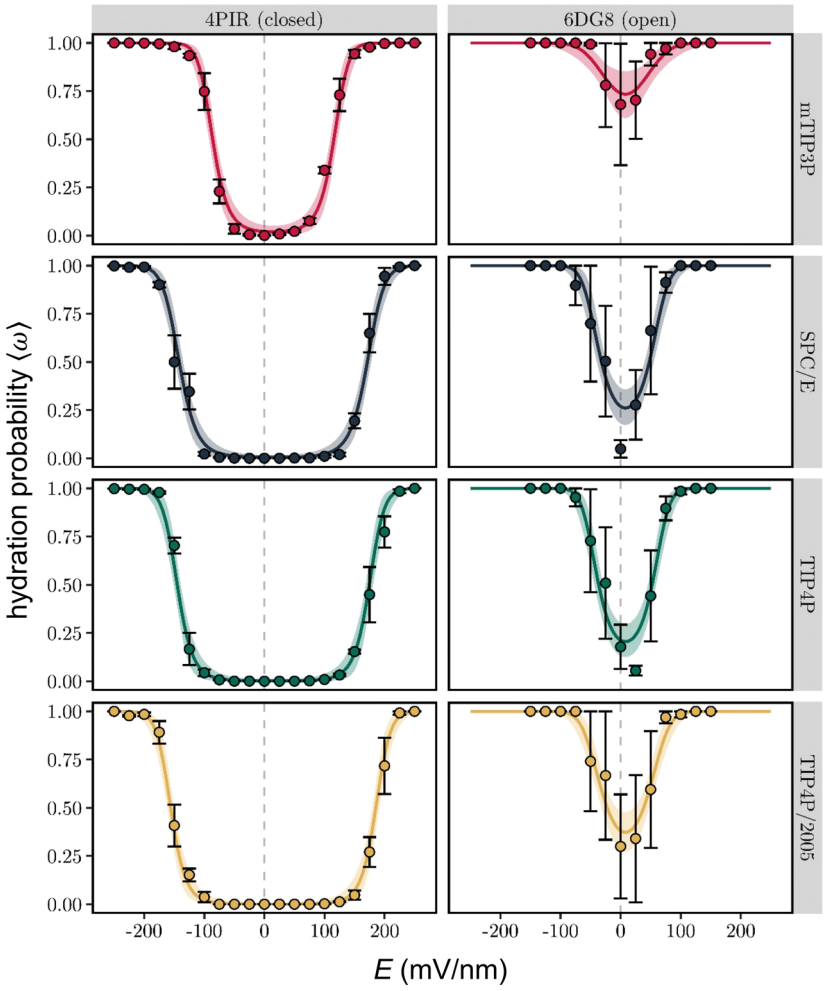

Figure 3. Hydration probability $\langle\omega\rangle$ as a function of the external electric field, E. Discrete data points and error bars represent the mean hydration probability and its standard error over three independent simulations, respectively. Solid lines are the result of a Bayesian nonlinear multilevel model (equation given above the figure and in the main text) fitted to the data (see Table 1 and SI Figure S3 for fitted parameters). The shaded area indicates the 95% confidence interval of the fit. Simulations were performed on the M2 helix nanopore from the closed (PDB ID: 4PIR) and open (PDB ID: 6DG8) conformations of the 5-HT$_3$ receptor and employed four different water models.

Table 1. Bayesian Estimates of Parameters for a Model of Pore Hydration Probability as a Function of E-Field[a]

PDB ID	water model	$\Delta\Omega_0$ (k_BT)	m (k_BT nm^2 V^{-2})	E_{INT} (mV nm^{-1})
4PIR	mTIP3P	−4.03 ± 0.68	396 ± 67	14.8 ± 1.4
4PIR	SPC/E	−5.51 ± 0.88	225 ± 36	
4PIR	TIP4P	−6.47 ± 1.32	253 ± 52	
4PIR	TIP4P/2005	−7.08 ± 1.31	243 ± 45	
6DG8	mTIP3P	1.03 ± 0.34	436 ± 171	7.9 ± 2.0
6DG8	SPC/E	−1.06 ± 0.25	668 ± 139	
6DG8	TIP4P	−1.37 ± 0.28	695 ± 126	
6DG8	TIP4P/2005	−0.53 ± 0.23	571 ± 122	

[a]Values listed represent the mean and standard deviation of the posterior distributions shown in SI Figure S3. The zero-field free energy difference, $\Delta\Omega_0$, electric field coupling, m, and intrinsic electric field, E_{INT}, are defined in the main text.

other three models have an approximately −1 k_BT preference for the vapor state. In marked contrast, all water models strongly favor the vapor state in the closed conformation, with zero-field free energy differences ranging from −4 to −6 k_BT. Notably, values using the mTIP3P model appear closest to the liquid state for both conformations. The strength of the coupling, m, between the hydration state of the pore and the electric field is also dependent on the conformation of the receptor. Apart from the mTIP3P water model, this parameter is more than twice as large for the open state than for the closed state. This difference may be attributed to the increased pore radius of the open conformation, which corresponds to a larger volume of water within the pore. There appears to be no clear trend for how m varies across water models. However, it should be noted that this parameter is sensitive to intermediate values of openness ($\langle\omega\rangle \approx 0.5$) and therefore may be affected by the larger error bars found in the transitional regime.

The horizontal offset to more positive potentials of the hydration probability is quantified by E_{INT}. In the closed conformation, E_{INT} is 14.8 ± 1.4 mV/nm. This reduces to 8.0

https://dx.doi.org/10.1021/acsnano.0c04387
ACS Nano XXXX, XXX, XXX−XXX

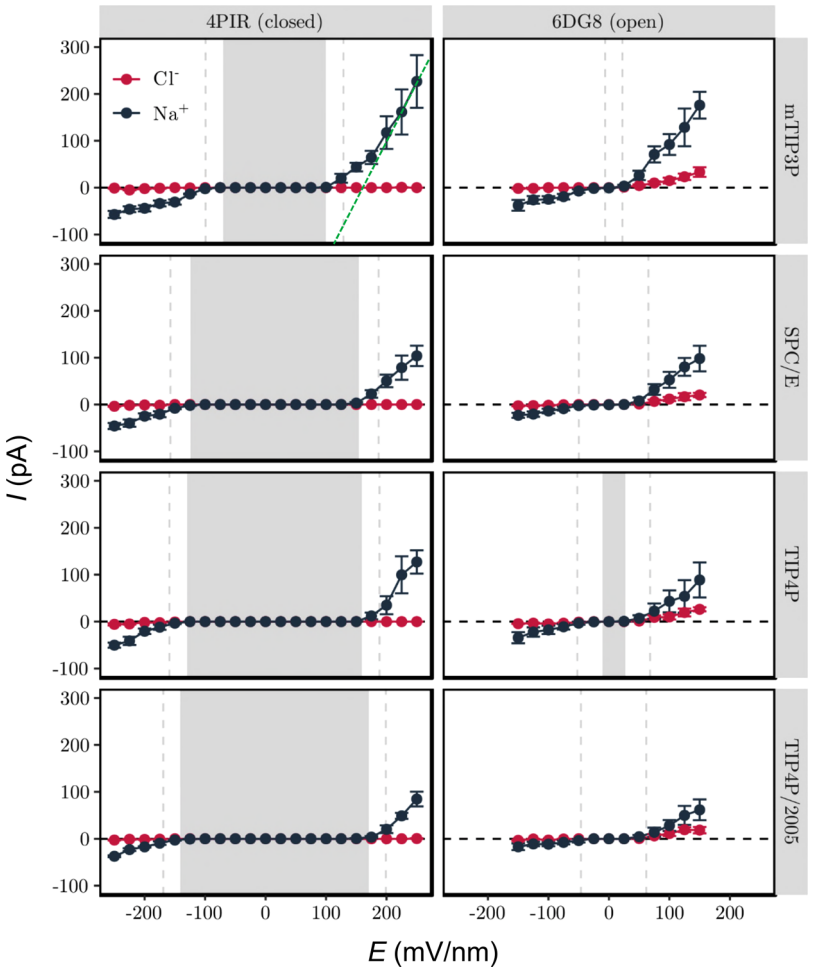

Figure 4. Ionic current through the 5-HT$_3$ receptor M2 helix nanopore in dependence of the external electric field. Background shading indicates the regime where the hydrophobic gate is mostly dewetted ($\langle\omega\rangle$ <0.25), while the vertical dashed lines indicate the transition to a mostly hydrated ($\langle\omega\rangle$ > 0.75) pore. The green dotted lines shown for the mTIP3P closed state plot represent the limiting Ohmic conductance (G_{max}) at high *E*-field (see text for further details).

± 2.0 mV/nm in the open conformation. Due to the sign convention this intrinsic field points from the extracellular to the intracellular domain. It therefore adds to the effective magnitude of an inward pointing external field ($E < 0$), while effectively reducing the impact of an outward pointing external field ($E > 0$). In this thermodynamic model, the shifting parameter, E_{INT}, is associated with the electric field arising from the charged amino acids of the channel protein, *i.e.*, the intrinsic electric field of the 5-HT$_3$ receptor M2 bundle. This was demonstrated by determining the electrostatic potential of the M2 bundle of the closed conformation by numerically solving the Poisson−Boltzmann equation (SI Figure S2A). The overall shape of the resultant electrostatic potential profile indicates that there is a substantial potential gradient between the intra- and extracellular openings of the M2 helix bundle, from −160 mV in the intracellular mouth well (IC in SI Figure S2) to −100 mV in the extracellular well (EC in SI Figure S2, when a lipid bilayer is included in the calculation). This corresponds to an electric field of 20 mV/nm, which is close to the E_{INT} value of ∼15 mV/nm found from the fit (Table 1). The relative distribution of charged amino acids (SI Figure S2B) therefore provides a molecular explanation of the resultant electrostatic profile, which could be explored further *via* channel perturbing mutations.

Ion Conduction through the Nanopore. In addition to determining the influence of the electric field on pore hydration, we also measured the resultant ion conduction through the channel (Figure 4; also SI Figure S4). For the closed (i.e., dehydrated) state the current due to either ion species (i.e., Na^+ or Cl^-) is approximately zero at low electric fields and begins to increase in magnitude only when the field exceeds the critical value required to hydrate the hydrophobic gate. Following this initial nonlinearity, the current then increases linearly with field strength for large electric fields. This implies that once the pore is hydrated, it acts as an Ohmic resistance. For the open state, the conductance is approximately Ohmic at lower field strengths (>50 mV/nm) reflecting the greater hydration of the pore. Interestingly, if we calculate the slope conductance at the highest field strengths (*i.e.*, $G_{max} = dI/dV$ at $E = +200$ mV/nm) for both the closed and open states, these values of G_{max} are of comparable magnitude. For example, for the mTIP3P water model the values of G_{max} (for sodium ions) for both the open and closed states are in the range 250 to 300 pS (derived from the data presented in Figure 4; note that there is a relatively high uncertainty associated with the conductance estimate given the error bars on the high field current estimates in this figure). This suggests that once this model nanopore is fully

https://dx.doi.org/10.1021/acsnano.0c04387
ACS Nano XXXX, XXX, XXX−XXX

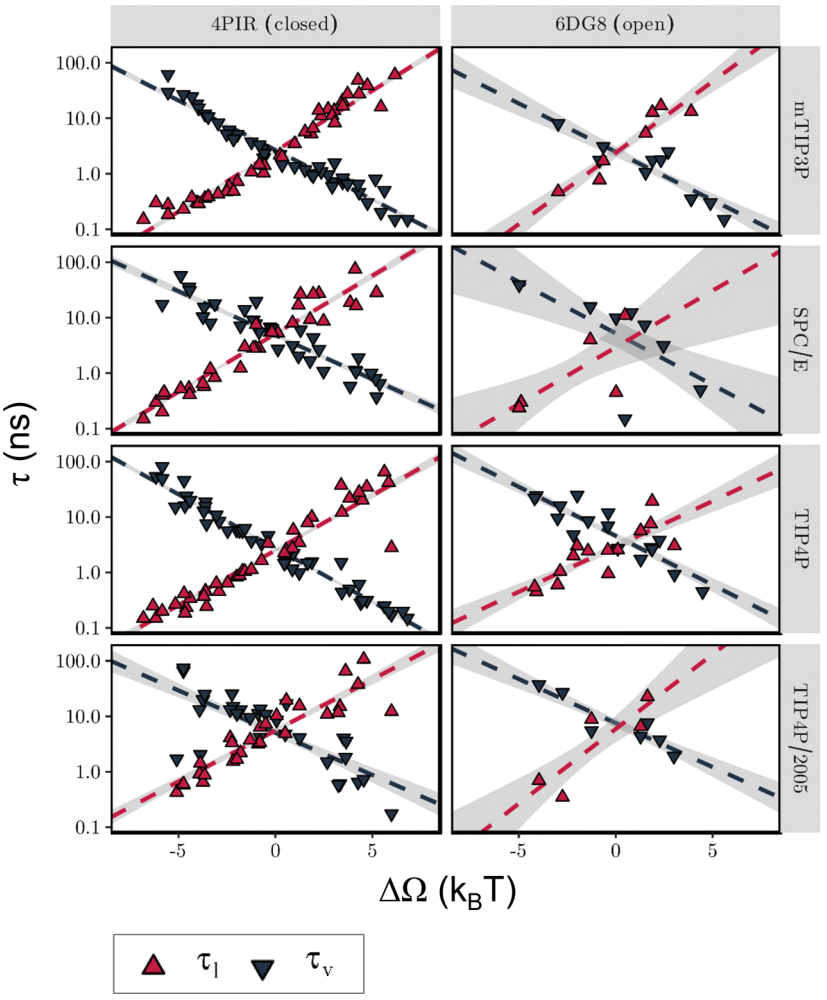

Figure 5. Kinetics of liquid−vapor transitions under the influence of an external electric field. The dependence of the mean survival times of the liquid (τ_l, red) and vapor (τ_v, black) states on the free energy difference ($\Delta\Omega$) between these states is shown. Each data point corresponds to an individual simulation, while the dashed line represents a linear fit to all data points, with confidence bands indicated as a shaded background. The free energy difference was estimated from the mean hydration probability, while the survival times were determined from the time series of hydration probability. Simulations with fewer than two observed transitions are not included in this plot.

hydrated and at relatively high *E*-fields, the overall shape and size of the pore dominates the limiting conductance, as discussed in early theoretical treatments of ion channel conductance.[51] Importantly, these results also indicate that pore dewetting prevents the formation of an ionic current in the closed state. This in turn implies that ion permeation itself does not cause pore hydration, given that the threshold field strength for hydration is dependent on the water model. This is supported by previous simulations of model nanopores, both highly simplified[31] and based on a β-barrel protein architecture.[38] In each case, imposition (*via* ionic concentration imbalance) of an electrostatic field across a hydrophobic nanopore first resulted in electrowetting of the pore. This was then *followed* by ion permeation; *i.e.*, water enters the pore first, to be followed at a later stage (in both cases within <1 ns) by ion permeation. Subsequently, while in the electrowetted state, there were periods of several nanoseconds when the pore remained fully wetted, but no ions were present within or passed through the model nanopore. Furthermore, in each case dissipation of the electric field by movement of ions through the pore resulted in subsequent dewetting of the pore. Overall, these observations support the conclusion that the transbilayer *E*-field itself causes pore hydration, which in turn enables ion permeation, rather than *vice versa*.

The value of G_{max} from our simulations exceeds ∼100 pS (Figure 4) which is more than 2 orders of magnitude greater than the physiologically observed single channel conductance (∼1 pS).[52] However, this difference likely reflects both the high *E*-field strength used in these simulations and also the absence of the intracellular and extracellular domains of the protein, which reduce the conductance substantially. Nevertheless, the Na^+ current is significantly larger than the Cl^- current. For example, for the open state with the mTIP3P water model, the G_{max} ratio for Na:Cl is >5; for the closed channel the corresponding ratio is substantially higher. This is in agreement with the cation selectivity of the 5-HT_3 receptor.[53] This is most likely due to the negatively charged residues near the intracellular (D−4′, E−1′) and extracellular (D20′) openings of the M2 helix bundle (SI Figure S2B), which make entry of Cl^- ions into the pore highly unfavorable, while remaining attractive for Na^+.

Kinetics of Liquid−Vapor Transitions. Having shown that an external *E*-field influences the hydration probability of a nanopore by changing the free energy difference between its liquid and vapor states, we next explored how the free energy

https://dx.doi.org/10.1021/acsnano.0c04387
ACS Nano XXXX, XXX, XXX−XXX

difference is controlled by the underlying rate constants. The kinetics of liquid−vapor transitions inside a hydrophobic gate can be examined in terms of the mean survival times of the liquid state, τ_l, and vapor state, τ_v, as they vary with the free energy difference between these two states. In Figure 5 it can be seen that τ_l grows exponentially with $\Delta\Omega$, while τ_v decreases exponentially at approximately the same rate. This trend is seen for both the closed and open states of the nanopore channel and across all four water models.

The lines in Figure 5 necessarily cross one another at $\Delta\Omega = 0$, as an equal probability for both states implies equal survival times. The crossover point thus defines a characteristic time scale for liquid−vapor transitions, which for the M2 helix nanopore has a value of $\tau_{lv} = \tau_l(\Delta\Omega = 0) = \tau_v(\Delta\Omega = 0) \approx 5$ ns. Importantly, this value is nearly identical for both the closed and the open states of the nanopore, despite their different pore radii. Furthermore, $\Delta\Omega = 0$ occurs at very different magnitudes of the electric field. This indicates that a time scale of ∼5 ns is likely to characterize liquid−vapor transitions of all pores that share the characteristic dimensions and surface hydrophobicity of the M2 helix nanopore considered here. A systematic survey of a range of nanopore models (see, *e.g.*, refs 7 and 54) could reveal how this time scale may depend on channel properties. Such slow behavior (water has a typical H-bond lifetime on the order of picoseconds) indicates these oscillations arise collectively, reminiscent of, *e.g.*, ultraslow reorientation of water wires with nanotubes[55] or in extended networks at the surface of a protein.[56] There is some slight variation of this oscillation time scale τ_{lv} across water models, but it always falls in the range between 1 and 10 ns, indicating a limited force field sensitivity.

This also suggests that a total simulation time, which is an order of magnitude larger than the characteristic time scale (i.e., 10 $\tau_{lv} \approx 50$ ns or above), is sufficient to characterize the hydration equilibrium behavior of the M2 helix nanopore systems. It is also worthwhile to compare the duration of the liquid and vapor states with the typical dwell times of the ions inside the channel pore (SI Figure S5). For ions that pass the closed conformation in its partially hydrated state ($\langle\omega\rangle = 0.25$ to 0.75), the average dwell time is comparable to the typical time scale of liquid−vapor transitions ($\tau_{lv} \approx 5$ ns). This implies that the intermittent periods during which the channel exists in the liquid state last sufficiently long enough to allow the passage of individual ions. For the open state, the typical ion dwell time lies below ∼1 ns. This is less than the average lifetime of the liquid state, which exceeds ∼1 ns. Consequently, even though most water models predict some degree of dehydration of the open state nanopore in the absence of an electric field (Figure 3), this state is still expected to allow the regular passage of ions and so is in agreement with our previous annotation of this structure as a functionally open state.[41]

CONCLUSIONS

In summary, we have shown that a transbilayer electric field can induce wetting of the hydrophobic gate of a model nanopore derived from the 5-HT_3 receptor. However, a field strength of ∼100 mV nm^{-1} is required to start to hydrate the pore of the closed conformation of the channel. This corresponds to a potential difference of ∼0.9 V, i.e., substantially greater than the transmembrane voltage an ion channel would normally experience under physiological conditions. We also present a simple model which can quantitatively describe the observed increase in pore hydration probability with increasing electric field, with the asymmetry of the hydration probability response curve accounted for by an offset parameter, E_{INT}, linked to the intrinsic electric field generated by the unequal distribution of charged amino acid residues along the length of the pore.

It is also useful to reflect on possible extensions to the current studies. One possibility would to be extend the comparison of water models to include polarizable models.[42] However, as yet for, *e.g.*, AMOEBA[57,58] external *E*-fields are not available in the GPU-accelerated OpenMM toolkit,[59,60] because the external-field-induced-dipole interaction is not implemented. Furthermore, it is likely that anisotropic atomic polarizability of the water molecule[61] may be needed for more accurate treatment of electrowetting. Another possible extension to this work would be to explore electrowetting in a complete protein channel. This would be computationally demanding, but would be of interest, *e.g.*, in terms of how a more complex distribution of charge within a protein might influence E_{INT}.

The finding that the threshold voltage required for hydrating a hydrophobic gate depends on the orientation of the electric field also provides an attractive perspective for the design of artificial nanopores. Our results suggest that an excess of only five elementary charges (from amino acid side chains) near one opening of the pore is sufficient to create a substantial intrinsic electric field acting in the transmembrane direction. Therefore, by functionalizing the openings of a hydrophobic pore with static charges,[62] it should be possible to design a nanopore that permits ion transport in only one direction, thus rectifying ionic currents. Importantly, this rectifying property would apply not only to ions but also to water molecules. This not only extends the concept of the electric-field induced smart water gates[63] but may also enable the creation of membrane systems that are semipermeable to water in a switchable fashion.

METHODS

Molecular Dynamics Simulations. MD simulations employing a constant electric field were performed in GROMACS 2018[64] using the protocols described below. Protein structures were obtained from the PDB and missing atoms were added using WHAT IF.[65] A 100 ns long MD simulation using the MARTINI force field[66] of the M2 helix bundle nanopore together with DOPC lipids and water was used to place the nanopore in a lipid bilayer.[67] During this coarse-grained simulation lipid molecules self-assemble into a bilayer structure around the protein. Following the self-assembly simulation, the protein−bilayer system was converted back to an atomistic representation and was solvated in a 0.15 M NaCl solution. The system was then equilibrated through a 10 ns long MD simulation employing the mTIP3P water model[49] and the CHARMM36m force field.[68,69]

Constant Electric Field Simulations. Production simulations were carried out using the CHARMM36m protein force field[68] and associated lipid parameters[68,69] in conjunction with the mTIP3P,[49] SPC/E,[70] TIP4P[49] or TIP4P/2005[50] water models. During these simulations, the effect of an external electric field, *E*, was modeled through an additional force, q_iE, acting on each atomic partial charge, q_i. The electric field was applied in the *z*-direction perpendicular to the plane of the membrane. Figure 2A illustrates this simulation setup.

It has been shown[47] that under periodic boundary conditions the application of an external field as described above is equivalent to the application of a transmembrane voltage, such that the voltage drop across the membrane is given by $\Delta V = -EL_z$, where L_z is the length of

https://dx.doi.org/10.1021/acsnano.0c04387
ACS Nano XXXX, XXX, XXX−XXX

the unit cell in the z-direction. For the system considered here $L_z \approx 8.5$ nm.

The magnitude of the electric field, E, was varied in steps of 25 mV nm^{-1} between −250 mV nm^{-1} and 250 mV nm^{-1} for the closed state structure (PDB ID: 4PIR) and between −150 mV nm^{-1} and 150 mV nm^{-1} for the open state structure (PDB ID: 6DG8). In terms of transmembrane potential, this corresponds to a step size of 0.2125 V and maximum transmembrane voltages of ±2.125 V and ±1.275 V, respectively. In each case, the range was chosen to ensure that a complete transition from a (partially) dewetted to a fully hydrated pore could be observed.

Preliminary simulations were carried out to assess the stability of the simulation system under electric fields of this magnitude. In order to assess pore hydration properties under high-field ($|E|$ > 150 mV nm−1) conditions (under which conditions electroporation may occur[71]), a harmonic restraining force of 1000 kJ mol^{-1} nm^{-2} was placed on the heavy atoms of all lipid molecules (after the initial 10 ns long equilibration period), which prevented electroporation.

Simulation Details. Three independent simulations of duration 150 ns for the closed conformation (PDB ID: 4PIR) and 50 ns for the open conformation (PDB ID: 6DG8) were carried out at each value of the electric field. Time integration was performed using a leapfrog integrator with a step size of 2 fs. Covalent bonds to hydrogen atoms were constrained using the LINCS algorithm,[72] and water model geometry was enforced using the SETTLE method.[73] The conformation of the protein was maintained close to its experimentally determined structure through the application of a harmonic restraining potential of 1000 kJ mol^{-1} nm^{-2} to all Cα atoms.

Long-range electrostatic interactions were treated through the smooth PME method[74] employing a real space cutoff of 1.0 nm and a Fourier spacing of 0.12 nm, with charge interpolation onto the grid through fourth order B-splines. Lennard-Jones interactions were switched off between 1.0 and 1.2 nm, and a long-range dispersion correction was applied to energy and pressure. All simulations were carried out in the isothermal isobaric (NPT) ensemble. The temperature was maintained at 310 K through a velocity rescaling thermostat[75] with a coupling constant of 0.1 ps, while a pressure of 1.0 bar was enforced through a semi-isotropic Parinello-Rahman barostat[76] with a coupling constant of 1.0 ps and a compressibility of 4.5×10^{-5} bar^{-1}.

Analysis. Unless otherwise specified, MD trajectories were postprocessed using MDAnalysis version 0.19.0[77] while further data analysis and visualization were performed through custom scripts written in the R language (https://www.r-project.org/). Molecular visualizations were created in VMD.[78]

As discussed above, the electrowetting of hydrophobic gates can be understood by considering the influence of an external electric field on the free energy difference between the liquid and vapor states of the pore (eq 2 above). Consequently, the hydration probability can be written as

$$\langle \omega \rangle = \frac{1}{1 + \exp[-\beta(\Delta\Omega_0 + m(E - E_{INT})^2)]}$$

which constitutes a nonlinear model with three free parameters, namely, $\Delta\Omega_0$ (the free energy difference in the absence of an external electric field), m (which represents how strongly the probability of hydration is coupled to the electric field), and E_{INT} (the horizontal offset accounting for the intrinsic electric field due to the protein; see above for more detailed discussion).

A fit of this equation to the observed hydration probability was obtained within the framework of Bayesian multilevel modeling.[79] Both $\Delta\Omega_0$ and m were treated as dependent on both the channel structure and water model, while E_{INT} was considered to only depend on the channel structure. The zero-field free energy difference, $\Delta\Omega_0$, may take both negative and positive values, and a Gaussian prior with mean $\mu = 0$ and standard deviation $\sigma = 10\ k_BT$ was used. In contrast to this, the coupling strength, m, is positive definite by definition. A gamma prior with shape $\alpha = 2$ and rate $\beta = 0.01$ was chosen to enforce this constraint, and sampling for this parameter was limited to positive values. While the intrinsic electric field, E_{INT}, can in principle be both positive and negative, allowing this parameter to vary over the entire real range caused divergent transitions in the sampling process. Sampling for this parameter was therefore restricted to positive values (in accordance with the observed data), and a gamma prior with shape $\alpha = 2$ and rate $\beta = 100$ was chosen.

The model was implemented in the probabilistic programming language Stan[80] through the brms[81] library in R. Posterior samples were generated through a Hamiltonian Monte Carlo[82,83] procedure using the No-U-Turn (NUTS) sampler.[84] For each of 10 independent Markov Chains, 10 000 warm-up and 10 000 sampling iterations were carried out. The NUTS sampler used a target average acceptance ratio of 0.9 and a maximum tree depth of 15.

ASSOCIATED CONTENT

Supporting Information

The Supporting Information is available free of charge at https://pubs.acs.org/doi/10.1021/acsnano.0c04387.

Methodological details and SI Figures S1−S5, showing electrowetting of the hydrophobic gate in the 5-HT$_3$ receptor comparing four water models; electrostatic potential of the M2 helix bundle of the closed state 5-HT$_3$ receptor; posterior probability of the Bayesian model parameters; cumulative charge flow through the M2 helix bundle of the closed state 5-HT$_3$ receptor (PDB ID: 4PIR) due to Na$^+$ ions; and dwell time of ions inside the M2 helix nanopore as a function of the E-field strength (PDF)

AUTHOR INFORMATION

Corresponding Authors

Mark S. P. Sansom − *Department of Biochemistry, University of Oxford, Oxford OX1 3QU, United Kingdom;* orcid.org/0000-0001-6360-7959; Email: mark.sansom@bioch.ox.ac.uk

Stephen J. Tucker − *Clarendon Laboratory, Department of Physics and OXION Initiative in Ion Channels and Disease, University of Oxford, Oxford OX1 3PU, United Kingdom;* orcid.org/0000-0001-8996-2000; Email: stephen.tucker@physics.ox.ac.uk

Author

Gianni Klesse − *Department of Biochemistry and Clarendon Laboratory, Department of Physics, University of Oxford, Oxford OX1 3QU, United Kingdom*

Complete contact information is available at: https://pubs.acs.org/10.1021/acsnano.0c04387

Notes

The authors declare no competing financial interest.

There is a preprint submission of this work: Electric Field Induced Wetting of a Hydrophobic Gate in a Model Nanopore Based on the 5-HT$_3$ Receptor Channel. *BioRxiv*, 2020, 2020.05.25.114157; https://www.biorxiv.org/content/10.1101/2020.05.25.114157v1 (accessed July 15th, 2020).

ACKNOWLEDGMENTS

This work was supported by the BBSRC (BB/N000145/1), EPSRC (EP/R004722/1), HECBioSim (EP/R029407/1), and the Wellcome Trust (208361/Z/17/Z). Our thanks to Shanlin Rao and Charlotte Lynch for their interest in and helpful comments on this work.

https://dx.doi.org/10.1021/acsnano.0c04387
ACS Nano XXXX, XXX, XXX−XXX

REFERENCES

(1) He, Z. J.; Zhou, J.; Lu, X. H.; Corry, B. Bioinspired Graphene Nanopores with Voltage-Tunable Ion Selectivity for Na^+ and K^+. *ACS Nano* **2013**, *7*, 10148−10157.

(2) Thomas, M.; Corry, B. Modifying Water Flow, Ion Selectivity, and Salt Rejection in Carbon Nanotubes *via* Surface Adsorption. *J. Phys. Chem. C* **2020**, *124*, 3820−3826.

(3) Thiruraman, J. P.; Masih Das, P.; Drndic, M. Ions and Water Dancing through Atom-Scale Holes: A Perspective toward "Size Zero". *ACS Nano* **2020**, *14*, 3736−3746.

(4) Lynch, C.; Rao, S.; Sansom, M. S. P. Water in Biological Channels and Nanopores: A Molecular Simulation Perspective *Chem. Rev.* **2020**, in press.

(5) Gouaux, E.; MacKinnon, R. Principles of Selective Ion Transport in Channels and Pumps. *Science* **2005**, *310*, 1461−1465.

(6) Zhu, Z. P.; Wang, D. Y.; Tian, Y.; Jiang, L. Ion/Molecule Transportation in Nanopores and Nanochannels: From Critical Principles to Diverse Functions. *J. Am. Chem. Soc.* **2019**, *141*, 8658−8669.

(7) Beckstein, O.; Sansom, M. S. P. Liquid−Vapor Oscillations of Water in Hydrophobic Nanopores. *Proc. Natl. Acad. Sci. U. S. A.* **2003**, *100*, 7063−7068.

(8) Beckstein, O.; Sansom, M. S. P. The Influence of Geometry, Surface Character and Flexibility on the Permeation of Ions and Water through Biological Pores. *Phys. Biol.* **2004**, *1*, 42−52.

(9) Rao, S.; Klesse, G.; Stansfeld, P. J.; Tucker, S. J.; Sansom, M. S. P. A Heuristic Derived from Analysis of the Ion Channel Structural Proteome Permits the Rapid Identification of Hydrophobic Gates. *Proc. Natl. Acad. Sci. U. S. A.* **2019**, *116*, 13989−13995.

(10) Beckstein, O.; Biggin, P. C.; Sansom, M. S. P. A Hydrophobic Gating Mechanism for Nanopores. *J. Phys. Chem. B* **2001**, *105*, 12902−12905.

(11) Allen, R.; Hansen, J. P.; Melchionna, S. Molecular Dynamics Investigation of Water Permeation through Nanopores. *J. Chem. Phys.* **2003**, *119*, 3905−3919.

(12) Jensen, M. O.; Borhani, D. W.; Lindorff-Larsen, K.; Maragakis, P.; Jogini, V.; Eastwood, M. P.; Dror, R. O.; Shaw, D. E. Principles of Conduction and Hydrophobic Gating in K^+ Channels. *Proc. Natl. Acad. Sci. U. S. A.* **2010**, *107*, 5833−5838.

(13) Zhu, F. Q.; Hummer, G. Drying Transition in the Hydrophobic Gate of the GLIC Channel Blocks Ion Conduction. *Biophys. J.* **2012**, *103*, 219−227.

(14) Aryal, P.; Sansom, M. S. P.; Tucker, S. J. Hydrophobic Gating in Ion Channels. *J. Mol. Biol.* **2015**, *427*, 121−130.

(15) Amiri, S.; Tai, K.; Beckstein, O.; Biggin, P. C.; Sansom, M. S. P. The α7 Nicotinic Acetylcholine Receptor: Molecular Modelling, Electrostatics, and Energetics. *Mol. Membr. Biol.* **2005**, *22*, 151−162.

(16) Corry, B. An Energy-Efficient Gating Mechanism in the Acetylcholine Receptor Channel Suggested by Molecular and Brownian Dynamics. *Biophys. J.* **2006**, *90*, 799−810.

(17) Beckstein, O.; Sansom, M. S. P. A Hydrophobic Gate in an Ion Channel: The Closed State of the Nicotinic Acetylcholine Receptor. *Phys. Biol.* **2006**, *3*, 147−159.

(18) Zhu, F. Q.; Hummer, G. Pore Opening and Closing of a Pentameric Ligand-Gated Ion Channel. *Proc. Natl. Acad. Sci. U. S. A.* **2010**, *107*, 19814−19819.

(19) Basak, S.; Gicheru, Y.; Rao, S.; Sansom, M. S. P.; Chakrapani, S. Cryo-EM Reveals Two Distinct Serotonin-Bound Conformations of Full-Length 5-HT_{3a} Receptor. *Nature* **2018**, *563*, 270−274.

(20) Polovinkin, L.; Hassaine, G.; Perot, J.; Neumann, E.; Jensen, A. A.; Lefebvre, S. N.; Corringer, P.-J.; Neyton, J.; Chipot, C.; Dehez, F.; Schoehn, G.; Nury, H. Conformational Transitions of the Serotonin 5-HT_3 Receptor. *Nature* **2018**, *563*, 275−279.

(21) Aryal, P.; Abd-Wahab, F.; Bucci, G.; Sansom, M. S. P.; Tucker, S. J. A Hydrophobic Barrier Deep within the Inner Pore of the TWIK-1 K2P Potassium Channel. *Nat. Commun.* **2014**, *5*, 4377.

(22) Jia, Z.; Yazdani, M.; Zhang, G.; Cui, J.; Chen, J. Hydrophobic Gating in BK Channels. *Nat. Commun.* **2018**, *9*, 3408.

(23) Neale, C.; Chakrabarti, N.; Pomorski, P.; Pai, E. F.; Pomes, R. Hydrophobic Gating of Ion Permeation in Magnesium Channel CorA. *PLoS Comput. Biol.* **2015**, *11*, No. e1004303.

(24) Yamashita, M.; Yeung, P. S. W.; Ing, C. E.; McNally, B. A.; Pomes, R.; Prakriya, M. Stim1 Activates Crac Channels through Rotation of the Pore Helix to Open a Hydrophobic Gate. *Nat. Commun.* **2017**, *8*, 14512.

(25) Chugunov, A. O.; Volynsky, P. E.; Krylov, N. A.; Nolde, D. E.; Efremov, R. G. Temperature-Sensitive Gating of Trpv1 Channel as Probed by Atomistic Simulations of Its Trans- and Juxtamembrane Domains. *Sci. Rep.* **2016**, *6*, 33112.

(26) Zheng, W.; Hu, R. K.; Cai, R. Q.; Hofmann, L.; Hu, Q. L.; Fatehi, M.; Long, W. T.; Kong, T.; Tang, J. F.; Light, P.; Flockerzi, V.; Cao, Y.; Chen, X. Z. Identification and Characterization of Hydrophobic Gate Residues in TRP Channels. *FASEB J.* **2018**, *32*, 639−653.

(27) Zheng, W.; Yang, X. Y.; Hu, R. K.; Cai, R. Q.; Hofmann, L.; Wang, Z. F.; Hu, Q. L.; Liu, X.; Bulkley, D.; Yu, Y.; Tang, J. F.; Flockerzi, V.; Cao, Y.; Cao, E. H.; Chen, X. Z. Hydrophobic Pore Gates Regulate Ion Permeation in Polycystic Kidney Disease 2 and 2L1 Channels. *Nat. Commun.* **2018**, *9*, 2302.

(28) Kasimova, M. A.; Yazici, A.; Yudin, Y.; Granata, D.; Klein, M. L.; Rohacs, T.; Carnevale, V. Ion Channel Sensing: Are Fluctuations the Crux of the Matter? *J. Phys. Chem. Lett.* **2018**, *9*, 1260−1264.

(29) Powell, M. R.; Cleary, L.; Davenport, M.; Shea, K. J.; Siwy, Z. S. Electric-Field-Induced Wetting and Dewetting in Single Hydrophobic Nanopores. *Nat. Nanotechnol.* **2011**, *6*, 798−802.

(30) Xie, G. H.; Li, P.; Zhao, Z. J.; Zhu, Z. P.; Kong, X. Y.; Zhang, Z.; Xiao, K.; Wen, L. P.; Jiang, L. Light- and Electric-Field-Controlled Wetting Behavior in Nanochannels for Regulating Nanoconfined Mass Transport. *J. Am. Chem. Soc.* **2018**, *140*, 4552−4559.

(31) Dzubiella, J.; Allen, R. J.; Hansen, J. P. Electric Field-Controlled Water Permeation Coupled to Ion Transport through a Nanopore. *J. Chem. Phys.* **2004**, *120*, 5001−5004.

(32) Dzubiella, J.; Hansen, J. P. Electric-Field-Controlled Water and Ion Permeation of a Hydrophobic Nanopore. *J. Chem. Phys.* **2005**, *122*, 234706.

(33) Daub, C. D.; Bratko, D.; Leung, K.; Luzar, A. Electrowetting at the Nanoscale. *J. Phys. Chem. C* **2007**, *111*, 505−509.

(34) Bratko, D.; Daub, C. D.; Leung, K.; Luzar, A. Effect of Field Direction on Electrowetting in a Nanopore. *J. Am. Chem. Soc.* **2007**, *129*, 2504−2510.

(35) Rant, U. Water Flow at the Flip of a Switch. *Nat. Nanotechnol.* **2011**, *6*, 759−760.

(36) Spronk, S. A.; Elmore, D. E.; Dougherty, D. A. Voltage-Dependent Hydration and Conduction Properties of the Hydrophobic Pore of the Mechanosensitive Channel of Small Conductance. *Biophys. J.* **2006**, *90*, 3555−3569.

(37) Sotomayor, M.; Vasquez, V.; Perozo, E.; Schulten, K. Ion Conduction through MscS as Determined by Electrophysiology and Simulation. *Biophys. J.* **2007**, *92*, 886−902.

(38) Trick, J. L.; Song, C.; Wallace, E. J.; Sansom, M. S. P. Voltage Gating of a Biomimetic Nanopore: Electrowetting of a Hydrophobic Barrier. *ACS Nano* **2017**, *11*, 1840−1847.

(39) Vaitheeswaran, S.; Rasaiah, J. C.; Hummer, G. Electric Field and Temperature Effects on Water in the Narrow Nonpolar Pores of Carbon Nanotubes. *J. Chem. Phys.* **2004**, *121*, 7955−7965.

(40) Maricq, A. V.; Peterson, A. S.; Brake, A. J.; Myers, R. M.; Julius, D. Primary Structure and Functional Expression of the $5HT_3$ Receptor, a Serotonin Gated Ion Channel. *Science* **1991**, *254*, 432−437.

(41) Trick, J. L.; Chelvaniththilan, S.; Klesse, G.; Aryal, P.; Wallace, E. J.; Tucker, S. J.; Sansom, M. S. P. Functional Annotation of Ion Channel Structures by Molecular Simulation. *Structure* **2016**, *24*, 2207−2216.

(42) Klesse, G.; Rao, S.; Tucker, S. J.; Sansom, M. S. P. Induced Polarization in Molecular Dynamics Simulations of the 5-HT_3 Receptor Channel. *J. Am. Chem. Soc.* **2020**, *142*, 9415−9427.

https://dx.doi.org/10.1021/acsnano.0c04387
ACS Nano XXXX, XXX, XXX−XXX

(43) Hassaine, G.; Deluz, C.; Grasso, L.; Wyss, R.; Tol, M. B.; Hovius, R.; Graff, A.; Stahlberg, H.; Tomizaki, T.; Desmyter, A.; Moreau, C.; Li, X.-D.; Poitevin, F.; Vogel, H.; Nury, H. X-Ray Structure of the Mouse Serotonin 5-HT_3 Receptor. *Nature* **2014**, *512*, 276−281.
(44) Crozier, P. S.; Henderson, D.; Rowley, R. L.; Busath, D. D. Model Channel Ion Currents in NaCl-Extended Simple Point Charge Water Solution with Applied-Field Molecular Dynamics. *Biophys. J.* **2001**, *81*, 3077−3089.
(45) Aksimentiev, A.; Heng, J. B.; Timp, G.; Schulten, K. Microscopic Kinetics of DNA Translocation through Synthetic Nanopores. *Biophys. J.* **2004**, *87*, 2086−2097.
(46) Aksimentiev, A.; Schulten, K. Imaging α-Hemolysin with Molecular Dynamics: Ionic Conductance, Osmotic Permeability, and the Electrostatic Potential Map. *Biophys. J.* **2005**, *88*, 3745−3761.
(47) Gumbart, J.; Khalili-Araghi, F.; Sotomayor, M.; Roux, B. Constant Electric Field Simulations of the Membrane Potential Illustrated with Simple Systems. *Biochim. Biophys. Acta, Biomembr.* **2012**, *1818*, 294−302.
(48) Vaitheeswaran, S.; Yin, H.; Rasaiah, J. C.; Hummer, G. Water Clusters in Nonpolar Cavities. *Proc. Natl. Acad. Sci. U. S. A.* **2004**, *101*, 17002−17005.
(49) Jorgensen, W. L.; Chandrasekhar, J.; Madura, J. D.; Impey, R. W.; Klein, M. L. Comparison of Simple Potential Functions for Simulating Liquid Water. *J. Chem. Phys.* **1983**, *79*, 926−935.
(50) Abascal, J. L. F.; Vega, C. A General Purpose Model for the Condensed Phases of Water: TIP4P/2005. *J. Chem. Phys.* **2005**, *123*, 234505.
(51) Kuyucak, S.; Chung, S. H. Temperature Depedence of Conductivity in Electrolyte Solutions and Ionic Channels of Biological Membranes. *Biophys. Chem.* **1994**, *52*, 15−24.
(52) Hussy, N.; Lukas, W.; Jones, K. A. Functional-Properties of a Cloned 5-Hydroxytryptamine Ionotropic Receptor Subunit - Comparison with Native Mouse Receptors. *J. Physiol.* **1994**, *481*, 311−323.
(53) Thompson, A. J.; Lummis, S. C. R. A Single Ring of Charged Amino Acids at One End of the Pore Can Control Ion Selectivity in the 5-HT_3 Receptor. *Br. J. Pharmacol.* **2003**, *140*, 359−365.
(54) Altabet, Y. E.; Debenedetti, P. G. Communication: Relationship between Local Structure and the Stability of Water in Hydrophobic Confinement. *J. Chem. Phys.* **2017**, *147*, 241102.
(55) Chakraborty, S.; Kumar, H.; Dasgupta, C.; Maiti, P. K. Confined Water: Structure, Dynamics, and Thermodynamics. *Acc. Chem. Res.* **2017**, *50*, 2139−2146.
(56) Zhang, L. Y.; Wang, L. J.; Kao, Y. T.; Qiu, W. H.; Yang, Y.; Okobiah, O.; Zhong, D. P. Mapping Hydration Dynamics around a Protein Surface. *Proc. Natl. Acad. Sci. U. S. A.* **2007**, *104*, 18461−18466.
(57) Ren, P. Y.; Ponder, J. W. Temperature and Pressure Dependence of the AMOEBA Water Model. *J. Phys. Chem. B* **2004**, *108*, 13427−13437.
(58) Laury, M. L.; Wang, L. P.; Pande, V. S.; Head-Gordon, T.; Ponder, J. W. Revised Parameters for the AMOEBA Polarizable Atomic Multipole Water Model. *J. Phys. Chem. B* **2015**, *119*, 9423−9437.
(59) Eastman, P.; Swails, J.; Chodera, J. D.; McGibbon, R. T.; Zhao, Y. T.; Beauchamp, K. A.; Wang, L. P.; Simmonett, A. C.; Harrigan, M. P.; Stern, C. D.; Wiewiora, R. P.; Brooks, B. R.; Pande, V. S. OpenMM 7: Rapid Development of High Performance Algorithms for Molecular Dynamics. *PLoS Comput. Biol.* **2017**, *13*, No. e1005659.
(60) Harger, M.; Li, D.; Wang, Z.; Dalby, K.; Lagardere, L.; Piquemal, J. P.; Ponder, J.; Ren, P. Y. Tinker-Openmm: Absolute and Relative Alchemical Free Energies Using AMOEBA on GPUs. *J. Comput. Chem.* **2017**, *38*, 2047−2055.
(61) Das, A. K.; Demerdash, O. N.; Head-Gordon, T. Improvements to the AMOEBA Force Field by Introducing Anisotropic Atomic Polarizability of the Water Molecule. *J. Chem. Theory Comput.* **2018**, *14*, 6722−6733.
(62) Polster, J. W.; Acar, E. T.; Aydin, F.; Zhan, C.; Pham, T. A.; Siwy, Z. S. Gating of Hydrophobic Nanopores with Large Anions. *ACS Nano* **2020**, *14*, 4306−4315.
(63) Xiao, K.; Zhou, Y. H.; Kong, X. Y.; Xie, G. H.; Li, P.; Zhang, Z.; Wen, L. P.; Jiang, L. Electrostatic-Charge- and Electric-Field-Induced Smart Gating for Water Transportation. *ACS Nano* **2016**, *10*, 9703−9709.
(64) Abraham, M. J.; Murtola, T.; Schulz, R.; Páll, S.; Smith, J. C.; Hess, B.; Lindahl, E. GROMACS: High Performance Molecular Simulations through Multi-Level Parallelism from Laptops to Supercomputers. *SoftwareX* **2015**, *1−2*, 19−25.
(65) Vriend, G. Whatif - a Molecular Modeling and Drug Design Program. *J. Mol. Graphics* **1990**, *8*, 52−56.
(66) Monticelli, L.; Kandasamy, S. K.; Periole, X.; Larson, R. G.; Tieleman, D. P.; Marrink, S. J. The Martini Coarse Grained Force Field: Extension to Proteins. *J. Chem. Theory Comput.* **2008**, *4*, 819−834.
(67) Stansfeld, P. J.; Goose, J. E.; Caffrey, M.; Carpenter, E. P.; Parker, J. L.; Newstead, N.; Sansom, M. S. P. MemProtMD: Automated Insertion of Membrane Protein Structures into Explicit Lipid Membranes. *Structure* **2015**, *23*, 1350−1361.
(68) Huang, J.; Rauscher, S.; Nawrocki, G.; Ran, T.; Feig, M.; de Groot, B. L.; Grubmuller, H.; MacKerell, A. D. CHARMM36M: An Improved Force Field for Folded and Intrinsically Disordered Proteins. *Nat. Methods* **2017**, *14*, 71−73.
(69) Klauda, J. B.; Venable, R. M.; Freites, J. A.; O'Connor, J. W.; Tobias, D. J.; Mondragon-Ramirez, C.; Vorobyov, I.; MacKerell, A. D.; Pastor, R. W. Update of the Charmm All-Atom Additive Force Field for Lipids: Validation on Six Lipid Types. *J. Phys. Chem. B* **2010**, *114*, 7830−7843.
(70) Berendsen, H. J. C.; Grigera, J. R.; Straatsma, T. P. The Missing Term in Effective Pair Potentials. *J. Phys. Chem.* **1987**, *91*, 6269−6271.
(71) Tarek, M. Membrane Electroporation: A Molecular Dynamics Simulation. *Biophys. J.* **2005**, *88*, 4045−4053.
(72) Hess, B.; Bekker, H.; Berendsen, H. J. C.; Fraaije, J. G. E. M. LINCS: A Linear Constraint Solver for Molecular Simulations. *J. Comput. Chem.* **1997**, *18*, 1463−1472.
(73) Miyamoto, S.; Kollman, P. A. Settle: An Analytical Version of the SHAKE and RATTLE Algorithm for Rigid Water Models. *J. Comput. Chem.* **1992**, *13*, 952−962.
(74) Darden, T.; York, D.; Pedersen, L. Particle Mesh Ewald: An N. Log(N) Method for Ewald Sums in Large Systems. *J. Chem. Phys.* **1993**, *98*, 10089−10092.
(75) Bussi, G.; Donadio, D.; Parrinello, M. Canonical Sampling through Velocity Rescaling. *J. Chem. Phys.* **2007**, *126*, 014101.
(76) Parrinello, M.; Rahman, A. Polymorphic Transitions in Single-Crystals: A New Molecular-Dynamics Method. *J. Appl. Phys.* **1981**, *52*, 7182−7190.
(77) Michaud-Agrawal, N.; Denning, E. J.; Woolf, T. B.; Beckstein, O. MDAnalysis: A Toolkit for the Analysis of Molecular Dynamics Simulations. *J. Comput. Chem.* **2011**, *32*, 2319−2327.
(78) Humphrey, W.; Dalke, A.; Schulten, K. VMD: Visual Molecular Dynamics. *J. Mol. Graphics* **1996**, *14*, 33−38.
(79) Gelman, A.; Hill, J. Data Analysis Using Regression and Multilevel/Hierarchical Models; *Analytical Methods for Social Research*; Cambridge University Press: Cambridge, 2007.
(80) Carpenter, B.; Gelman, A.; Hoffman, M. D.; Lee, D.; Goodrich, B.; Betancourt, M.; Brubaker, M.; Guo, J. Q.; Li, P.; Riddell, A. STAN: A Probabilistic Programming Language. *J. Stat. Software* **2017**, *76*, 1−29.
(81) Burkner, P. C. BRMS: An R Package for Bayesian Multilevel Models Using STAN. *J. Stat. Software* **2017**, *80*, 1−28.
(82) Neal, R. M. MCMC Using Hamiltonian Dynamics. In *Handbook of Markov Chain Monte Carlo*; Handbooks of Modern Statistical Methods; Brooks, S., Gelman, A., Jones, G. L., Meng, X. L., Eds.; Chapman and Hall/CRC Press: Boca Raton, 2011; pp 113−162.

https://dx.doi.org/10.1021/acsnano.0c04387
ACS Nano XXXX, XXX, XXX−XXX

(83) Betancourt, M. A Conceptual Introduction to Hamiltonian Monte Carlo. *arXiv*; 1701.02434v2, 2017. https://arxiv.org/abs/1701.02434v2 (accessed July 15 2020).
(84) Hoffman, M. D.; Gelman, A. The No-U-Turn Sampler: Adaptively Setting Path Lengths in Hamiltonian Monte Carlo. *J. Machine Learning Res.* **2014**, *15*, 1593−1623.
(85) Klesse, G.; Rao, S.; Sansom, M. S. P.; Tucker, S. J. CHAP: A Versatile Tool for the Structural and Functional Annotation of Ion Channel Pores. *J. Mol. Biol.* **2019**, *431*, 3353−3365.

https://dx.doi.org/10.1021/acsnano.0c04387
ACS Nano XXXX, XXX, XXX−XXX